

The fusion process of successive droplets impinging onto a substrate surface

SuLi Li¹ · ZhengYing Wei¹ · Jun Du¹ · Pei Wei¹ · ZuoXian Hou¹ · BingHeng Lu¹

Received: 4 November 2014 / Accepted: 30 March 2015 / Published online: 18 April 2015
© Springer-Verlag Berlin Heidelberg 2015

Abstract Successive deposition of uniform metal droplet is a new kind of 3D printing and rapid prototyping technology. This paper presents a systematic numerical investigation of the transient transport phenomenon during the fusion of successive droplets impinging onto a substrate surface. The physical mechanisms of the fusion process, including the bulk liquid, capillarity effects at the liquid–solid interface, heat transfer, and solidification, are identified and quantified numerically. The 3D models based on a volume of fluid method were developed to investigate the successive deposition of molten metal droplets on a horizontally aluminum substrate surface. The numerical models are validated with experiments. The comparison between numerical simulations and experimental findings shows a good agreement. The effects of relative distances between two successive molten droplets on the end-shapes of impact regime are examined. This investigation is essential to implement effective process control in metal micro-droplet deposition manufacture.

1 Introduction

The 3D printing and rapid prototyping (RP) technology are applied more and more widely, including metal deposition manufacturing technology under different parameters of impinging, spreading, and fusion, which have got a wide

application in modern industry [1]. The 3D printing and rapid prototyping (RP) technology by successive deposition metal droplets are an additive process, and the components are manufactured from molten metal materials in a single operation without using any mold or other tooling. Near net shape parts are fabricated by sequentially depositing molten droplets layer by layer [2]. Up to now, the generation of molten metal droplets has been developed into two main modes: continuous jetting [3–8] and drop-on-demand (DOD) jetting [9, 10]. The former mode can produce high-frequency droplets with a piezoelectric ceramic actuator. However, it is difficult to control the fall position and temperature of the droplets compared with the second one. The second one has excellent controllability in the velocity, temperature, and diameter of the droplets, resulting in the extensive applications from the printing of electronic circuits to the fabrication of 3D components [11]. In the DOD mode, the molten metal in the crucible for jetting can be ejected out from a nozzle by heat, charge, or gas pulse. Among these, gas pulse readily generates metal droplets.

Currently, the simulation works related to droplet deposition and fusion processes were mainly based on 2D models, which focus on the normal impinging of single droplet onto a fixed substrate surface [12–21]. However, 2D models could not provide comprehensive details of the deposition process. Thus, a 3D model has been developed to study complex flows in the successive deposition process of droplets [22–25]. Ghafouri-Azar et al. [26] investigated the inter-impinging of two tin droplets with the diameter of millimeter scale and simulated the fusion behaviors of droplets. Furthermore, there are few reports on the successive droplets impinging on a substrate surface. Xu et al. [27] investigated the fusion process of droplets by assuming that the impinging droplets were pre-deformed into

✉ ZhengYing Wei
zywei@mail.xjtu.edu.cn

SuLi Li
lty818210@gmail.com

¹ The State Key Laboratory for Manufacturing Systems Engineering, Xi'an Jiaotong University, Xi'an 710049, China

cylindrical discs with a given thickness. The droplet morphology was considered as a disc after impacting with a substrate, and the fluid dynamics of spreading and fusion of droplets were neglected.

During the fabrication process of 3D components by DOD technique, droplets are deposited onto a horizontally moving aluminum substrate surface and fuse with each other to form a line and layer. However, successive deposition and solidification of molten metal droplets on the horizontally moving substrate have not been studied. In this paper, the successive deposition and solidification of molten aluminum droplets on a horizontally moving aluminum substrate were numerically simulated by the 3D model based on the volume of fluid (VOF) method. In order to confirm the implications of the numerical simulations, molten metal droplets were successively generated by the DOD jetting and deposited onto a horizontally moving substrate surface. The 3D images of morphology evolution of droplets were also discussed.

2 Modeling and analysis

The present study aims at developing a 3D model of successive deposition of uniform molten metal droplets on a horizontally moving substrate. So, the model consists of droplets (the first droplet, the second droplet, the third droplet, and the fourth droplet), a substrate, and air, as shown in Fig. 1. Several assumptions have been made as follows:

1. The droplets with spherical morphology are generated at a fixed velocity V .
2. The initial temperature distribution within droplets is uniform.
3. The substrate is horizontally moved at a constant velocity V_S .

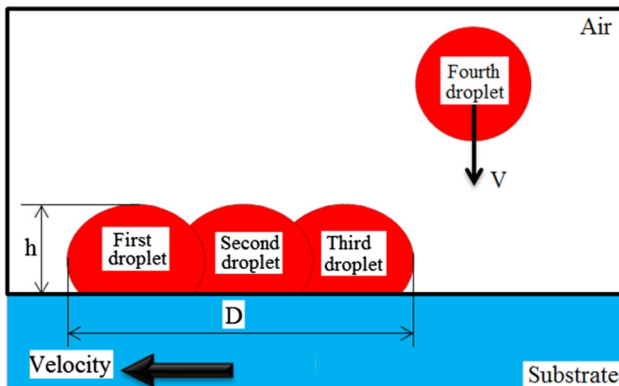


Fig. 1 Schematic representation of the mathematical model for successive droplet deposition

4. The surrounding gas is considered as a void region, and thus, the heat loss of droplets by convection and radiation is ignored.

A typical calculation mesh consists of approximately two million rectangular cells. The mesh has uniform grid spacing in x , y , and z directions, equal to 30 cells per diameter of the droplets [18].

2.1 Theoretical model

The successive droplet deposition processes are numerically simulated by solving 3D Navier–Stokes, continuity, and energy equations. The VOF technique is coupled with Navier–Stokes and energy equations to track the surface of the droplet on a fixed structured mesh [30, 31].

The fluid flow during the droplet spreading onto the substrate is modeled by using the Navier–Stokes equations for incompressible flows (Eqs. 1, 2):

$$\rho \frac{\partial V}{\partial t} + \rho(V \cdot \nabla)V = -\nabla P + \nabla \cdot \mu(\nabla V + (\nabla V)^T) + \rho g + F_{TS} + F \quad (1)$$

$$\nabla \cdot V = 0 \quad (2)$$

where V is the velocity, P is the pressure, ρ is the density and μ is the kinematic viscosity, and g is the gravitational acceleration. F is the term source corresponding to the occurrence of the droplet solidification, and F_{TS} represents the capillary forces given by (Eq. 3):

$$F_{TS} = \sigma \dot{m} \delta \dot{k} \quad (3)$$

where σ , δ , and m are the surface tension coefficient, the Dirac function, and the average local slope of the curve at the liquid–gas interface, respectively. k is the normal at the liquid–gas interface. Both fluids are assumed incompressible and Newtonian, and the surrounding air has no effect on the deposition process. Other assumptions are that the liquid is incompressible and the fluid flow is laminar.

2.2 Advection on the interface

To track and follow the evolution of the interface between the two fluids (metal droplet, and air), we have used the level set method [18], which has been proven popular in recent years for tracking, modeling, and simulating the motion of moving interfaces or boundaries. In this method, the interface is represented by a certain level set or iso-contour of a globally defined function, i.e., the level set function θ . This function θ is a smoothed step function that equals 0 in a domain and 1 in its complementary part. Across the interface, there is a smooth transition from 0 to 1 and the interface is represented implicitly by the 0.5 iso-

contour (Fig. 2). The interface moves with the fluid velocity v . This is described by the following equation:

$$\frac{\partial \theta}{\partial t} + v \nabla \theta = \eta \nabla \left(\varepsilon \nabla \theta - \theta (1 - \theta) \frac{\nabla \theta}{|\nabla \theta|} \right) \quad (4)$$

The terms of Eq. 4 give the correct motion of the interface. The parameters ε and η determine the thickness of the region and the amount of re-initialization or stabilization of the level set function, respectively. Any property α of the two fluids at the interface such as density, viscosity, or thermal conductivity may be expressed as:

$$\alpha = \alpha_{\text{gas}} + \theta(\alpha_{\text{liquid}} - \alpha_{\text{gas}}) \quad (5)$$

The process of spreading and solidification of a molten droplet impinging onto a solid surface involves fluid flow, heat transfer, and phase change. Complex phenomena involved are not thoroughly understood yet. For example, the interface between the droplet and the surrounding gas and between the liquid and solid phases remains a challenging problem to deal with for scientists and engineers.

2.3 Heat transfer and solidification

The heat exchange between the droplet, air, and substrate is modeled by using the energy equation (Eq. 6):

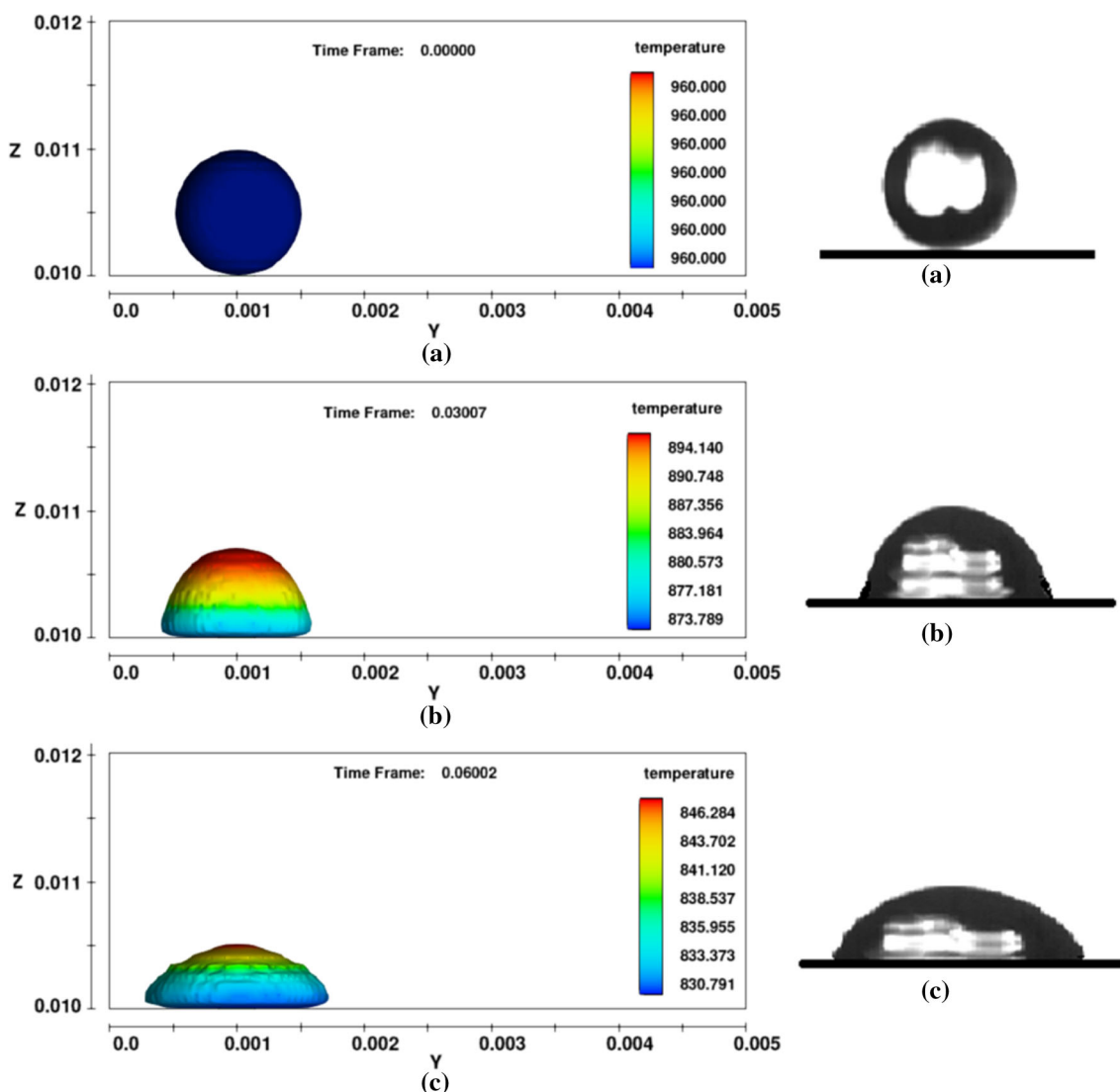


Fig. 2 Comparison of SEM photo and simulation results of a 1-mm-diameter aluminum alloy droplet impacting on an aluminum substrate: **a left** simulated morphology and temperature of the first droplet at 0 s; **a right** SEM photo of morphology of the first droplet at 0 s; **b left** simulated morphology and temperature of the first droplet

at 0.03007 s; **b right** SEM photo of morphology of the first droplet at 0.03007 s; **c left** simulated morphology and temperature of the first droplet at 0.06002 s; **c right** SEM photo of morphology of the first droplet at 0.06002 s

$$\rho C_p \frac{\partial T}{\partial t} + \nabla \cdot (-\lambda \nabla T) = -\rho C_p u \cdot \nabla T \quad (6)$$

where T , ρ , and C_p denote the droplet temperature, density, and specific heat, respectively. The thermal contact resistance is introduced to take into account the discontinuity of temperature at the interface due to the non-perfect contact between the droplet and the substrate. The thermal contact resistance (TCR) is modeled by defining a thin layer of arbitrary thickness L_0 . The effective thermal conductivity K_L for the splat is related to the TCR by Eq. 7:

$$K_L = \frac{L_0}{TCR} \quad (7)$$

As the hot droplet spreads on the cold substrate, it cools down and solidifies. Many approaches have been used for modeling solid/liquid transitions. The enthalpy porosity method shows a good ability for modeling some complex problems involving phase change as crystal grows from the melt [19–21]. The specific heat C_p in the energy equation Eq. 6 is replaced by:

$$C_p = C_{p\text{solide}} + \frac{\Delta H}{T_m} + \Delta H \cdot \delta \quad (8)$$

where f is a smooth Dirac delta function with nonzero values in a range of temperature equal to ΔT and its integration over temperature is equal to unity, ΔH the latent heat of the transition, and T_m the melting temperature. ΔT is the temperature gap between liquidus temperature ($T_m + \Delta T$) and solidus one ($T_m - \Delta T$), and δ is a Gaussian curve given by Eq. 9:

$$\delta = \frac{\exp(-(T - T_m)^2)/(\Delta T)^2}{\Delta T \sqrt{\pi}} \quad (9)$$

The source term in Eq. 1 is defined in Eq. 10 and serves to slow down the velocity of the fluid at the phase-change interface and eventually arrest its motion as the droplet cools down [22].

$$F = \frac{(1 - \beta)^2}{\beta^3 + \eta} \cdot C \cdot u \quad (10)$$

where β is the volume fraction of the liquid phase, given by Eq. 11:

$$\beta = \begin{cases} 0 & T < T_m - \Delta T \\ \frac{T - T_m + \Delta T}{2\Delta T} & T_m - \Delta T \leq T \leq T_m + \Delta T \\ 1 & T > T_m + \Delta T \end{cases} \quad (11)$$

In Eq. 10, C is the mushy zone constant (should have high value to produce a proper damping), η arbitrary constant (should have small value to prevent division by zero), and u is the spreading velocity of the splat [28, 29].

Through comparing the calculated spread factor from present model with the experimental value, a mushy zone constant of 10^4 – 10^7 was found to be more appropriate for simulation on the solidification problem occurring in low-speed impact and fusion process, instead of the range of 10^8 – 10^9 recommended [30, 31].

3 Experimental validation of the numerical model

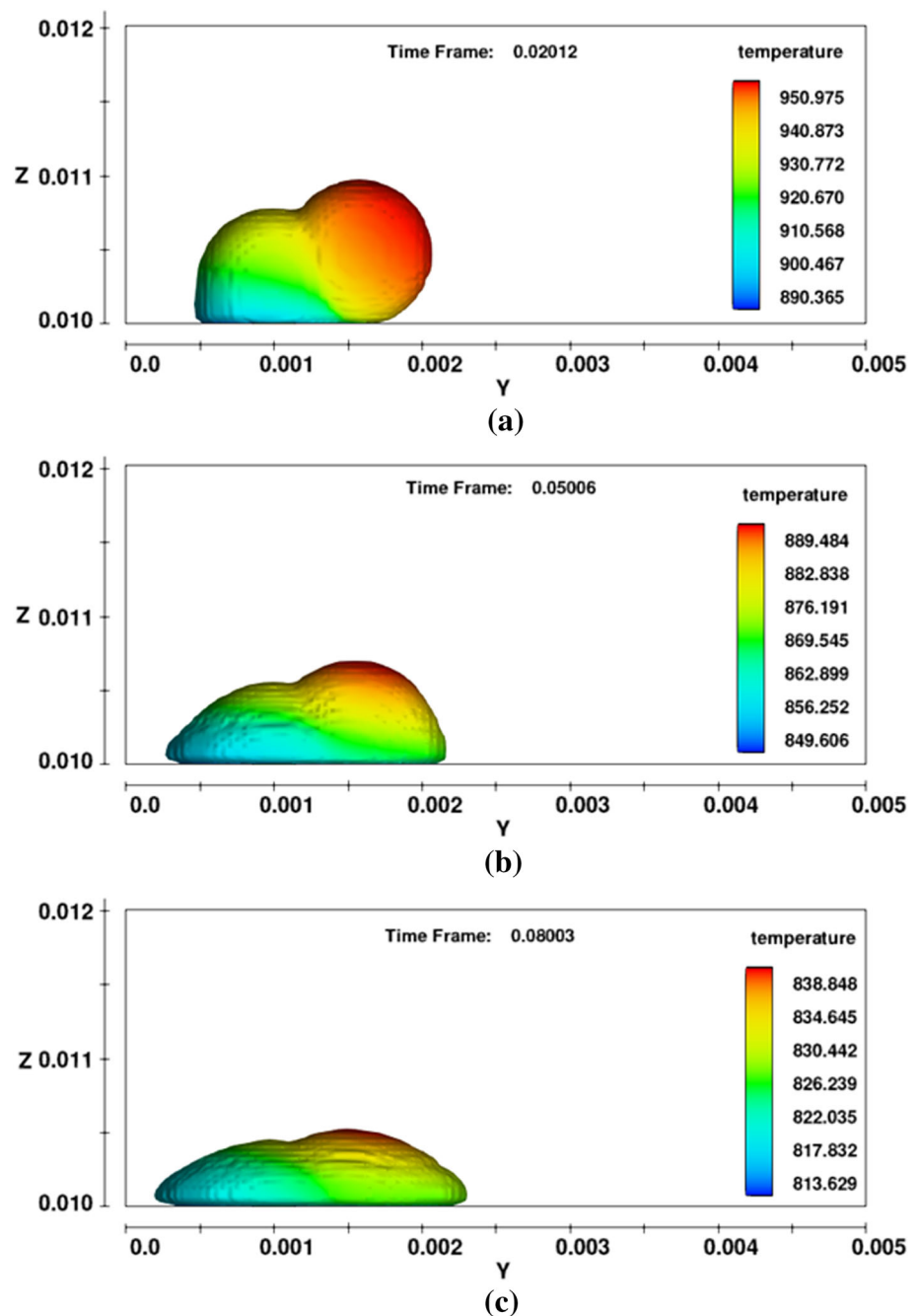
To validate the numerical model, experimental observation of the end-shapes of successive droplets was performed to compare and validate the numerical results. Aluminum alloy droplets having a diameter of 1 mm and an initial temperature of 935 K were generated with the DOD jetting and successively deposited onto an aluminum substrate; the relevant thermo-physical parameters of the molten droplet and the substrate material are listed in Table 1. Argon gas pulse was used as the driving force. A mass of 150 g aluminum alloy billet was placed in a graphite crucible. A spray nozzle with 0.5 mm diameter was located at the bottom of the crucible, which was built in a resistance furnace.

The initial conditions of the model in this study are listed in Tables 1, respectively. In this study, the substrate melting and solidification are not modeled. The contact angle, defined as the angle at which a droplet interface meets a solid surface, is assumed to be 90°. As reported by Pasandideh-Fard and Mostaghimi [17], the contact angle

Table 1 Process parameters of deposition experiments

Parameter	Value
Droplet material	Aluminum
Droplet density ($\rho/\text{kg m}^{-3}$)	2368
Droplet surface tension ($\sigma/\text{N m}^{-1}$)	0.8
Droplet melting point (T/K)	933
Droplet velocity ($V/\text{m s}^{-1}$)	1
Droplet temperature (T_d/K)	935
Substrate temperature (T_s/K)	300
Droplet diameter (d/mm)	1
Inlet pressure (P_s/MPa)	0.2
Deposition distance (H_s/mm)	10
Solidification angle ($\theta/^\circ$)	90
Substrate material	Aluminum
Substrate density ($\rho/\text{kg m}^{-3}$)	2700
Substrate heat capacity ($C_p/\text{J kg}^{-1} \text{K}^{-1}$)	900
Substrate diffusivity ($\alpha/\text{m}^2 \text{s}^{-1}$)	9.75e-5
Substrate thermal conductivity ($k/w \text{ m}^{-1} \text{K}^{-1}$)	237

Fig. 3 Simulation results of two 1-mm-diameter aluminum alloy droplets impacting on an aluminum substrate: **a** simulated morphology and temperature of the second droplet at 0.02012 s; **b** simulated morphology and temperature of the second droplet at 0.05006 s; **c** simulated morphology and temperature of the second droplet at 0.08003 s

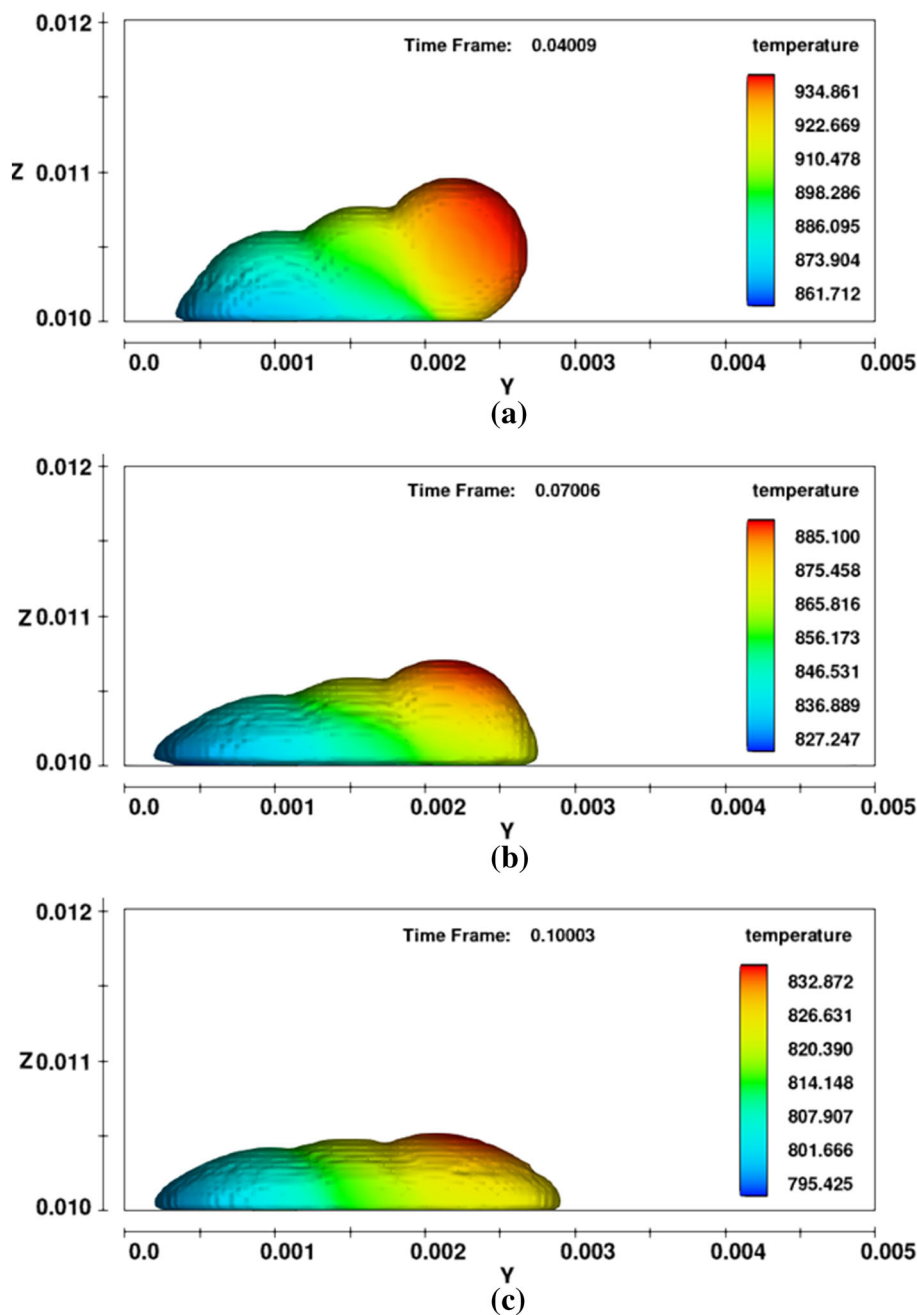


does not affect the splat spreading if the impact velocity is higher than 1 m/s.

Figure 2 shows the evolution of morphology and temperature of a 1-mm droplet impacting a substrate surface with a velocity of $V = 1$ m/s at different times (Fig. 2 left). It is observed that the droplet has been stuck to the substrate and dragged forward. The spreading diameter D showed a trend of increasing, the spreading height h showed a trend of reducing, and they are all unchanged after 0.2 s; this shows that the droplet has been completely frozen.

The results show good qualitative agreement with experimental photographs in the corresponding period (Fig. 2 right). The deposition experiment was performed in a glove box under an inert atmosphere with low oxygen content (no more than 150 ppm). Thus, the uniform molten droplets were ejected out of the nozzle. The distance from the nozzle to the substrate was 10 mm, where the morphology and dynamic behavior of the molten droplets tend to be stable. Once the droplet contacts the cold substrate, it is simultaneously cooled by means of heat transfer to the

Fig. 4 Simulation results of three 1-mm-diameter aluminum alloy droplets impacting on an aluminum substrate: **a** simulated morphology and temperature of the third droplet at 0.04009 s; **b** simulated morphology and temperature of the third droplet at 0.07006 s; **c** simulated morphology and temperature of third droplet at 0.10003 s



substrate and begins to solidify. That is, the base of the droplet initially solidifies and is stuck to the substrate.

4 Results and discussion

4.1 Deposition of the successive droplet

Figure 3 shows the morphology and temperature evolution of fusion between the first droplet and the second droplet. At the substrate velocity of 1 mm/s, the second one initially impinges the top right surface of the first droplet. Due

to the non heating of the substrate, the solidification forms bottom to top of the second droplet and the first droplet, which would result in some frozen layer at the contact area. This frozen layer is prejudice for metallurgical bonding between these two droplets. Because of the fusion between molten droplets, the interface between the two droplets will gradually decrease. Due to lack of enough support from the partially remelted droplet, the second droplet comes into contact with the substrate, increasing the area of heat dissipation for the second droplet. Thus, the heat carried by the second droplet transfers to the conjoint droplet, which is confirmed by the solidification of the second droplet.

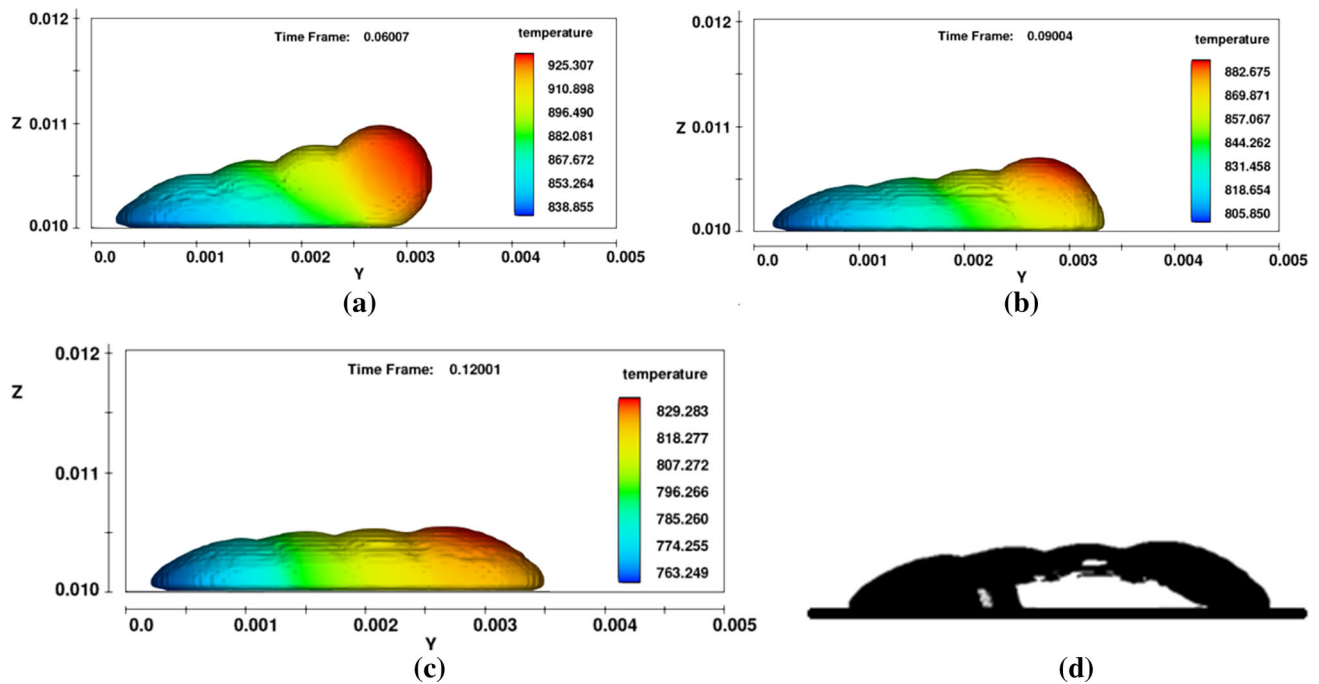


Fig. 5 Comparison of SEM photo and simulation results of four 1-mm-diameter aluminum alloy droplets impacting on an aluminum substrate: **a** simulated morphology and temperature of the fourth droplet at 0.06007 s; **b** simulated morphology and temperature of the

fourth droplet at 0.09004 s; **c** simulated morphology and temperature of the fourth droplet at 0.12001 s; **d** SEM photo of morphology of the fourth droplet at 0.12001 s

The third droplet closely resembles the second one in morphology and temperature evolution, as shown in Fig. 4. When the next droplet and the previous droplet began to fuse, its spreading diameter D increased rapidly, and spreading height h was still falling, because the second droplet was still not fully in contact with the substrate, which was still spreading and fusing. After the second droplet contacts with the substrate completely, the spreading diameter D and spreading height h are not changed.

Figure 5a–c shows 3D images of morphology and temperature evolution of the fourth droplet impinging onto a substrate with impact velocity of 1 m/s. In the pileup process, surface tension forces resist and viscous forces damp the spreading process. Concurrently, solidification influences the spreading process as well. The results show good qualitative agreement with experimental photographs at 0.12001 s (Fig. 5d).

When the next droplet comes in contact with the previous one (Figs. 3, 4, 5), if the previous droplet is incompletely solidified at this moment, then the melt of the previous one will merge with that of the next droplet; the melt after coalescence will continually spread under the action of the initial momentum of the next one. Therefore, it can be seen that the next droplet spreads more than the previous one at the initial contact stage. There are many ripples in the upper part of the solidified droplet. The ripples were the direct results of layered solidification

consisting of the alternate spreading and recoiling of the droplet. However, the whole pileup process was retained until the droplets completely solidified (Figs. 3, 4, 5). In metal droplet deposition manufacture, forming accuracy and quality can be directly reflected in the morphological characteristics and metallurgical defects (such as microvoid and cold lap) of the pileups, respectively. To obtain better quantitative results, four series of numerical experiments were performed to investigate the interactions between impacting droplets and the previous droplets (totally solidified or not), and the influence of the impact velocity, droplet size, and substrate temperature on the end-shapes of the pileup was analyzed.

4.2 The fusions between molten metal droplets

Figure 6 shows the time evolution of the change of droplets spreading diameter and height. It can be seen that it is divided into four areas, respectively: (1) the first metal molten droplet is dripping and spreading; (2) the second metal molten droplet is dripping and fusing with the first droplets; (3) the third metal molten droplet is dripping and fusing with the second droplets; (4) the fourth metal molten droplet is dripping and fusing with the third droplets.

Through the successive four droplets spreading and fusing with one and another, it can be seen that the eventually spreading height h after solidification of the four droplets is essentially the same. This explains that the

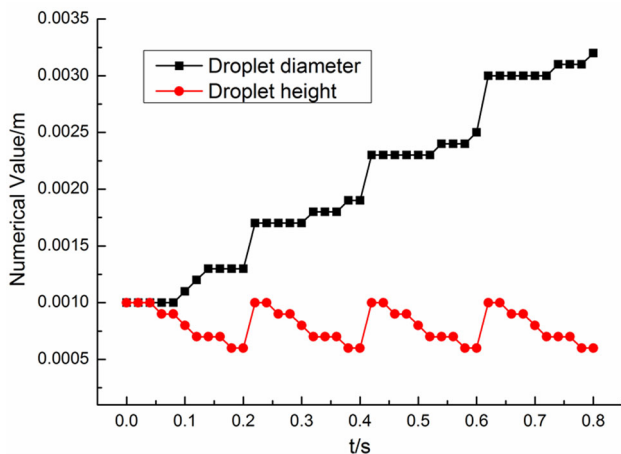


Fig. 6 Time evolution of the droplet height h and the diameter D

forming process is good, providing favorable conditions for forming the next floor. From the point of spreading diameter D , it increases a certain value when spreading out a single droplet. The basic value equals to the droplet diameter; this is associated with the moving velocity of substrate.

5 Conclusions

A 3D model for successive deposition of molten Al droplets onto a horizontally moving substrate was developed based on a VOF method. The simulations with this model could agree well with the experimental results and provide an insight into the spreading and fusion of molten Al droplets during successive deposition and yield following specific results.

1. In this DOD jetting, both simulated and experimental results demonstrate that deposited droplets have high-profile shape, which would be useful for the improvement in the efficiency and accuracy of UDJ technology.
2. Through the successive droplets spreading and fusing with one and another, it can be seen that the eventually spreading height h after solidification of the four droplets is essentially the same. This explains that the forming process is good, providing favorable conditions for forming the next floor.
3. In the process of deposition, the carrying heat of later deposition molten droplets makes partial remelt of the solidified surface, in order to realize the metallurgical combination between each other, which make the whole parts get some of the surface of the forming quality and precision. Therefore, the existences of the fusion line are the primary cause of crack formation and extend continuously, by adjusting the parameters

such as nozzle temperature, nozzle distance, and substrate temperature, and so on and can eliminate the metal fusion defect.

Acknowledgments The research is financially supported by the National Natural Science Foundation of China under Grant No. 31370944, the Natural Science Foundation of Shaanxi province (Grant 2014JQ7238), and China Postdoctoral Science Foundation (Grant 2014M560764).

References

1. F. Gao, A. Sonin, Proc. R. Soc. Lond. **444**, 533 (1994)
2. L.J. Zarzalejo, K.S. Schmaltz, C.H. Amon, Heat Mass Transf **34**, 477 (1999)
3. J.P. Kruth, Ann. CIRP **40**(2), 603 (1991)
4. M. Orme, J. Mater. Eng. Perform. **2**(3), 399 (1993)
5. M. Orme, C. Huang, J. Courte. Miner. Metals Mater. Soc., Warren dale, PA, 125(1996)
6. M.E. Orme, C. Huang, J. Courter, At. Sprays **6**, 305 (1996)
7. Q. Liu, M. Orem, J. Eng. Manuf. **215**(10), 1333 (2001)
8. C.H. Amon, K.S. Schmaltz, R. Merz et al., J. Heat Transf. **118**(1), 164 (1996)
9. M. Neagu, Technol. Mech. Eng. **5**, 35 (2004)
10. J.D. Benrardin, C.J. Stebbins, I. Mudawar, Int. J. Heat Mass Transf. **40**(2), 247 (1997)
11. G.E. Cossali, M. Marengo, M. Santini, Int. J. Heat Mass Transf. **29**, 167 (2008)
12. M. Pasandideh-Fard, S.D. Aziz, S. Chandra, J. Mostaghimi, Int. J. Heat Fluid Flow **22**, 201 (2001)
13. N. Nikolopoulos, A. Theodorakakos, G. Bergeles, Int. J. Heat Mass Transf. **50**, 303 (2007)
14. G. Strotos, M. Gavaises, Andreas, Int. J. Heat Mass Transf. **45**, 213 (2007)
15. J. Fukai, Y. Shiliba, Yanmaoto et al., Phys. Fluids **7**, 236 (1995)
16. L.J. Zarzalejo, K.S. Schmaltz, C.H. Amon, Int. J. Heat Mass Transf. **34**, 477 (1999)
17. S. Haferl, D. Poulidakos, J. Heat Mass Transf. **46**, 535 (2003)
18. Y.P. Chao, L.H. Qi et al., China Mech Eng **20**, 207 (2009)
19. M. Fang, S. Chandra, C.B. Park, J. Manuf. Sci. Eng. **129**, 311 (2007)
20. C. Escure, M. Vardelle, Plasma Chem. Plasma Process. **23**(2), 185 (2003)
21. J. Luo, L.H. Qi et al., Int. J. Mach. Tools Manuf. **48**, 289 (2008)
22. M. Fang, S. Chandra, C.B. Park, J. Heat Transf. **131**, 112101 (2009)
23. X.S. Jiang, L.H. Qi, J. Luo, H. Huang, J.M. Zhou, Int. J. Adv. Manuf. Technol. **49**, 535 (2010)
24. V. Butty, D. Poulidakos, J. Giannakouros, Int. J. Heat Fluid Flow **23**, 232 (2002)
25. S. Kamnis, S. Gu, T.J. Lu, C. Chen, J. Phys. D Appl. Phys. **41**, 165303 (2008)
26. R. Ghafouri-Azar, S. Shakeri, S. Chandra, J. Mostaghimi, Int. J. Heat Mass Transf. **46**, 1395 (2003)
27. Q. Xu, V.V. Gupta, E.J. Lavernia, Acta Mater. **48**, 835 (2000)
28. B. Kang, J. Waldvogel, D. Poulidakos, J. Mater. Sci. **30**, 4912 (1995)
29. R.K. Chin, J.L. Beuth, C.H. Amon, J. Manuf. Sci. Eng. **123**, 623 (2001)
30. S. Alavi, M. Pasandideh-Fard, Front. Heat Mass Transf. (FHMT) **2**, 023007 (2011)
31. Y.Z. Zheng et al., Appl. Surf. Sci. **317**, 526 (2014)